Linear Combination Steady-State Free Precession MRI

Shreyas S. Vasanawala,* John M. Pauly, and Dwight G. Nishimura

A new, fast, spectrally selective steady-state free precession (SSFP) imaging method is presented. Combining k-space data from SSFP sequences with certain phase schedules of radiofrequency excitation pulses permits manipulation of the spectral selectivity of the image. For example, lipid and water can be resolved. The contrast of each image depends on both T_1 and T_2, and the relative contribution of the two relaxation mechanisms to image contrast can be controlled by adjusting the flip angle. Several potential applications of the technique, referred to as linear combination steady-state free precession (LCSSFP), are demonstrated: fast musculoskeletal, abdominal, angiographic, and brain imaging. Magn Reson Med 43:82–90, 2000. © 2000 Wiley-Liss, Inc.

Key words: fast imaging; steady-state free precession; T_2 contrast; musculoskeletal imaging; abdominal imaging; magnetic resonance angiography; fat suppression; lipid suppression; linear combination steady-state free precession magnetic resonance; MRA; SSFP; FISP; MRI

Steady-state free precession (SSFP) methods, which refocus all gradients over a repetition interval, permit fast imaging with high signal, but suffer from banding artifacts due to B_0 inhomogeneity. Additionally, SSFP techniques yield an undesirably large lipid proton signal (1). Recently, we presented a solution addressing these issues called fluctuating equilibrium magnetic resonance (FEMR); a novel pulse sequence was described for producing a magnetization that fluctuates from excitation to excitation in the steady state, thus permitting the simultaneous acquisition of multiple images with differing spectral responses (1). In this article, we discuss another method of modifying the spectral response of SSFP imaging: reconstructing sundry images from linear combinations of Fourier data from several SSFP sequences, each image with a unique spectral response. We call this method linear combination SSFP (LCSSFP).

Briefly, the nonuniform spectral response of SSFP may serve as a novel tissue contrast generation mechanism. With the correct choice of sequence repetition time (TR), all spins within a certain spectral range are suppressed while all other protons yield high signal. Furthermore, by acquiring a complete Fourier dataset multiple times, each time with an SSFP sequence with a different radiofrequency (RF) phase schedule, and then linearly combining the datasets before reconstruction, the spectral profile of the resulting image intensity is modified. Specifically, the band of suppressed Larmor frequencies can be translated and broadened. Additionally, using a linear combination of SSFP data first proposed by Schwenk (2) and Zur et al. (3) the suppression band can be eliminated altogether.

By taking different linear combinations of the datasets, multiple images can then be reconstructed, each with a different spectral response. Two goals can thus be achieved. In particular, lipid and water can be resolved based on chemical shift differences. Since conventional lipid suppression techniques have hitherto been incompatible with an SSFP sequence, new applications of steady-state techniques are possible with this method and FEMR. Second, SSFP can be rendered immune to main field inhomogeneity artifacts. Several clinical applications of the technique are demonstrated in this article, including musculoskeletal and abdominal examples, brain imaging, and fast noncontrast-enhanced MR angiography.

MATERIALS AND METHODS

We now describe two manifestations of LCSSFP which we refer to as two-phase imaging and four-phase imaging. Techniques that rewind magnetization over a repetition interval have a long history in NMR spectroscopy (4), and though imaging sequences based on totally refocused techniques have been proposed and demonstrated over a decade ago (5–7), severe banding artifacts from field inhomogeneity precluded widespread clinical adoption (8). A standard SSFP sequence is depicted in Fig. 1. After every RF excitation, phase encode gradient and data acquisition, spins are completely rephased with refocusing gradients on all three axes. Thus, transverse coherences are maintained from one repetition interval to the next, and magnetization is utilized with optimal efficiency, yielding a high signal given by:

$$s + \frac{ae^{i\theta} + b}{c\cos\theta + d}$$

where θ is the precession phase over a TR, β is the flip angle, and we have $a = -(1 - E_1)E_2 \sin\beta$, $b = (1 - E_1)\sin\beta$, $c = E_2(E_1 - 1)(1 + \cos\beta)$, and $d = 1 - E_1\cos\beta - (E1 - \cos\beta)E_2^2$; $E_1 = e^{-\mathrm{TR}/\mathrm{T}_1}$, and $E_2 = e^{-\mathrm{TR}/\mathrm{T}_2}$.

The spectral response of the sequence depends on the excitation flip angle, with large flip angles yielding a large passband and a narrow stopband (Fig. 2), and small flip angles producing a narrow passband and a wide stopband (not shown). The banding artifacts alluded to in the Introduction are a manifestation of the stopband. Note that the plots in Fig. 2 show but one cycle of periodic responses; longer TRs permit greater magnetization precession between excitation pulses and, hence, a decrease in the period of the functions shown in Fig. 2. Thus, shortening repetition times decreases the number of artifactual bands within the field of view.

With the appropriate repetition time, the stopband described above will include the Larmor frequency of lipid

Magnetic Resonance Systems Research Laboratory, Department of Electrical Engineering, Stanford University, Stanford, California.

Grant sponsors: GE Medical Systems; NIH; Grant numbers: CA 50948; HL 39297; NS 29434.

*Correspondence to: Shreyas S. Vasanawala, Information Systems Laboratory, Packard 063, 350 Serra Mall, Stanford, CA 94305-9510.
E-mail: vasanawala@stanford.edu

Received 9 April 1999, revised 17 August 1999, accepted 18 August 1999.

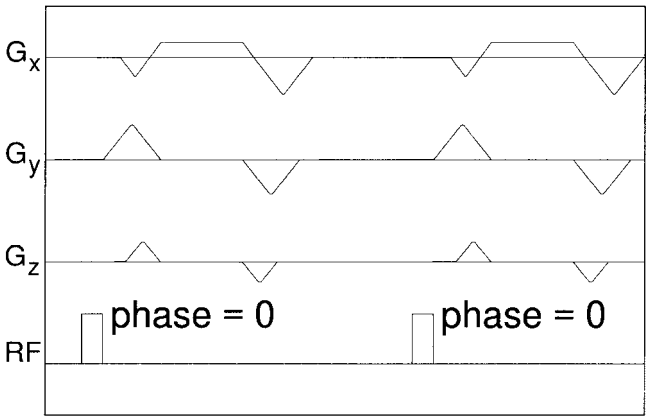

FIG. 1. Timing diagram for two phase encoding steps of a 3D free precession sequence. Note that magnetization is completely rewound over a TR. Although the two RF phases are zero in the diagram, a linearly increasing phase from excitation to excitation also constitutes an SSFP sequence.

spins, providing a new lipid suppression method. Unfortunately, with a narrow stopband (40 Hz at 1.5 T and 2.5 ms TR), the technique lacks robustness to field inhomogeneity. Additionally, the theoretical response of lipids varies from that obtained experimentally (1). Specifically, the experimental stopband is narrower than predicted and the signal has an unexpectedly high intensity at one edge of the stopband (Fig. 3). This is likely a variant of the so-called bright fat effect observed with fast-spin-echo sequences. The phenomenon occurs with rapid RF pulsing and is thought to be due to decoupling of methylene protons (9–11). Regardless of etiology, the phenomenon requires stringent constraints on main field uniformity for robust lipid suppression.

The saturation band in the spectral profile of SSFP methods plagues NMR applications, distorting resonance peaks. In this context, a solution was proposed by Schwenk (2), called Quadriga spectroscopy, and a modified version of that method by Ernst (12), called four-phase Fourier spectroscopy. Both solutions entail repeating the SSFP measurement four times, each time with a different RF carrier frequency or phase cycle, and then complexly summing the free induction decay signals. The resulting spectral profile has uniform magnitude and phase. A similar modification to SSFP imaging may be employed. Specifically, a full dataset is acquired with four SSFP sequences with RF excitation phase cycles: 0-0-0-0, 0-90-180-270, 0-180-0-180, and 0-270-180-90. Although k-space data from each imaging sequence can be reconstructed independently, the data from the four experiments is first complexly summed to generate new k-space data, which is then Fourier-transformed. The magnitude and phase of the resulting spectral profile is shown in Fig. 4.

Because of a longer scan time, the four-phase technique yields a higher SNR compared with that of standard SSFP imaging or FEMR imaging. As described in this article, the four-phase technique is less SNR-efficient than standard SSFP imaging by nearly 40% (Fig. 5), although a modification has been previously described that recovers the SNR efficiency of SSFP (3). For fluoroscopic imaging, although a compromised temporal response is inevitable, a sliding reconstruction window (13,14) results in an identical image frame rate as conventional sequences. Specifically, the four SSFP sequences are repeated indefinitely, and after a complete dataset is acquired with each sequence, an image is reconstructed with the most recently acquired four datasets.

Zur et al. (3) have shown that the signal in an SSFP sequence with RF phase increment of ϕ is a sum of echoes, each with a phase determined by the precession phase over a TR, θ, and is given by

$$D_\phi = \Sigma_n A_n e^{in\phi} e^{in\theta},$$

where A_n are echo amplitudes. Additionally, they described a technique for isolating the echoes. The isolation of A_0 is equivalent to the four-phase technique. Note that the echoes form basis functions and can be recombined to approximate a desired spectral response, $f(\theta)$. Denote the terms of a Fourier expansion of $f(\theta)$ as C_n: $f(\theta) = \Sigma_n C_n\, e^{in\theta}$. Then approximate the first few terms of the expansion as a combination of SSFP data with coefficients α_j:

$$\Sigma_n C_n e^{in\theta} = \Sigma_j \alpha_j D_{\phi_j} = \Sigma_j \alpha_j \Sigma_n A_n e^{in\phi_j} e^{in\theta}$$

Equating Fourier terms gives $C_n = \Sigma_j \alpha_j A_n\, e^{in\phi_j}$, and $\boldsymbol{\alpha} = \mathbf{L}^{-1}\mathbf{C}$, where $L_{nj} = A_n e^{in\phi_j}$. Thus, given a desired spectral response, a linear combination of SSFP data can be found to approximate it. However, since $\mathbf{L}$ depends on T_1, T_2, and the flip angle, the linear combination coefficients must be determined for the expected flip angle and a given T_1 and T_2. Then the spectral response must be checked for other T_1 and T_2 values.

As an example, a spectral response with a broad stopband can be designed. Using four RF phase increments of 0, 90, 180, and 270, the solution gives small coefficients for D_{90} and D_{270}. If we denote data from an SSFP sequence with a phase cycle of 0–0 (i.e., phase increment of 0) as D_{0-0}, and data from an SSFP sequence with phase cycle of 0–180 (i.e., phase increment of 180) as D_{0-180}, then $D_{0-0} + iD_{0-180}$ and $D_{0-0} - iD_{0-180}$ are solutions with relatively broad stopbands. Moreover, the spectra of the two solutions are

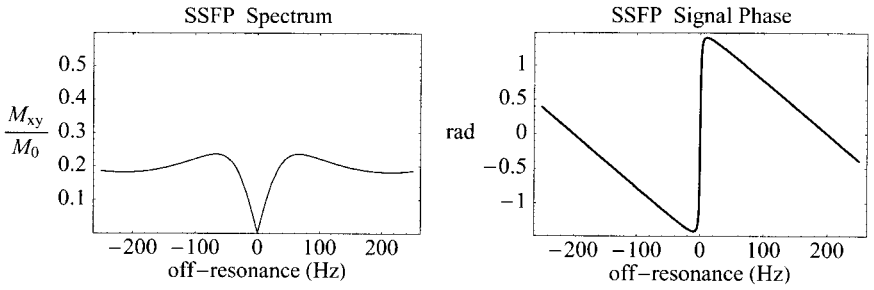

FIG. 2. SSFP equilibrium transverse magnetization magnitude (left) and phase (right) for a species with T_1 of 900 ms and T_2 of 200 ms (TR = 2.5 ms, 25° flip angle). Spins near the resonance frequency are saturated, so by shifting the RF frequency, a particular chemical species can be suppressed. The width of the passband and stopband inversely scale with the sequence repetition time.

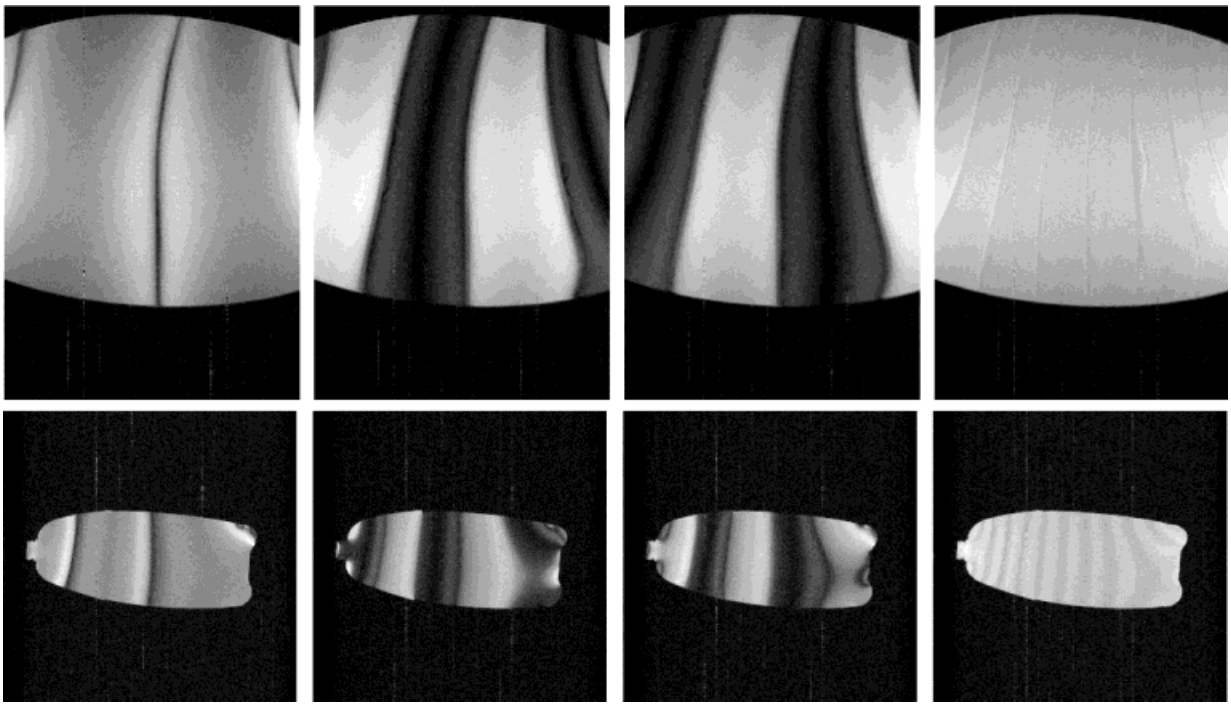

FIG. 3. Images of water (top) and lipid (bottom) phantoms acquired with a constant gradient field from the left to the right of the images. From left to right, images were acquired with data from an SSFP sequence, $D_{0-0} + iD_{0-180}$, $D_{0-0} - iD_{0-180}$, and $D_{0-0-0-0} + D_{0-90-180-270} + D_{0-180-0-180} + D_{0-270-180-90}$. For all sequences, a 45° excitation and 3.3 ms TR were employed. Note the relatively thin band of suppression with SSFP in the lipid image (left bottom image), and a broad region of high intensity just left of it. The high intensity band may be due to decoupling of methyl protons in lipid, and the consequent increase in T_2 relaxation time. The two-phase images (middle two) have much broader bands of signal suppression, as predicted by theoretical off-resonance equilibrium magnetization profiles, whereas the four-phase images have no suppression bands.

nearly orthogonal (Fig. 6). Thus, by acquiring two Fourier datasets, two images can be reconstructed using these two linear combinations of the data; one image is generated from spins within a certain band of resonance frequencies, and the other image from spins within another band of resonance frequencies. With the appropriate choice of repetition time (2.2 ms at 1.5 T), the centers of the two passbands can be placed 220 Hz apart: one image is then of predominantly water spins, while the other image is mainly lipid spins. Hence, we have a novel water-lipid separation method, which we refer to as a two-phase technique. Although twice the scan time is required compared with SSFP to achieve the lipid suppression, the SNR efficiency is not compromised compared with that of SSFP or FEMR imaging (Fig. 5). Note that the two-phase technique may be incorporated into four-phase imaging, simply by using the D_{0-0} and D_{0-180} datasets. Additionally, using the $D_{0-90-180-270}$ and $D_{0-270-180-90}$ datasets analogously to the D_{0-0} and D_{0-180} datasets yields similar spectral profiles that are shifted by a quarter period.

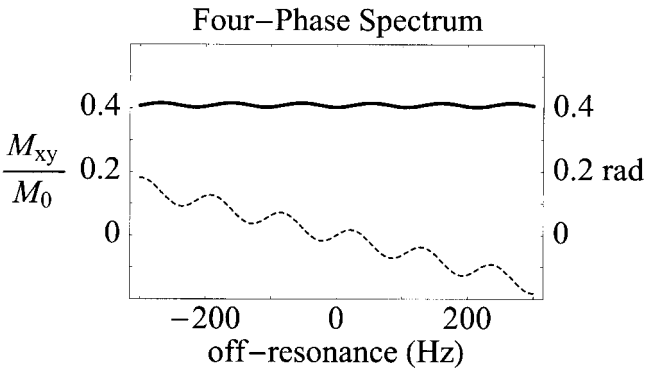

FIG. 4. Four-phase equilibrium signal magnitude (solid curve) and phase (dashed curve) for species with T_1 of 900 ms and T_2 of 100 ms (TR = 2.5 ms, 25° flip angle). The spectrum, which has a period that scales inversely with the TR, is fairly uniform, compared with that of SSFP. Thus, when the TR is decreased to prevent large phase variations of the response within a single voxel, there should be no banding artifacts in images acquired with the four-phase method.

LCSSFP has similar T_1 and T_2 contrast properties as SSFP; signal is proportional to T_2/T_1, as shown in Fig. 7. Note that the relative contribution of T_2 relaxation effects to the image contrast can be controlled through the flip angle, which is better appreciated in Fig. 8.

RESULTS

We now present experimental verification of the predicted behavior of the LCSSFP methods, followed by some applications. All studies employed a GE Signa 1.5 T scanner. To ascertain the spectral response of the sequences, 2D field maps of water and lipid (soybean oil) phantoms were acquired with a continual shim field gradient applied in one direction (Fig. 3) which generated a spatially varying Larmor frequency. Then, also with a continual shim field gradient, the phantoms were imaged with SSFP and LCSSFP sequences. Registering the images with the field maps then permitted derivation of the spectral response of the se-

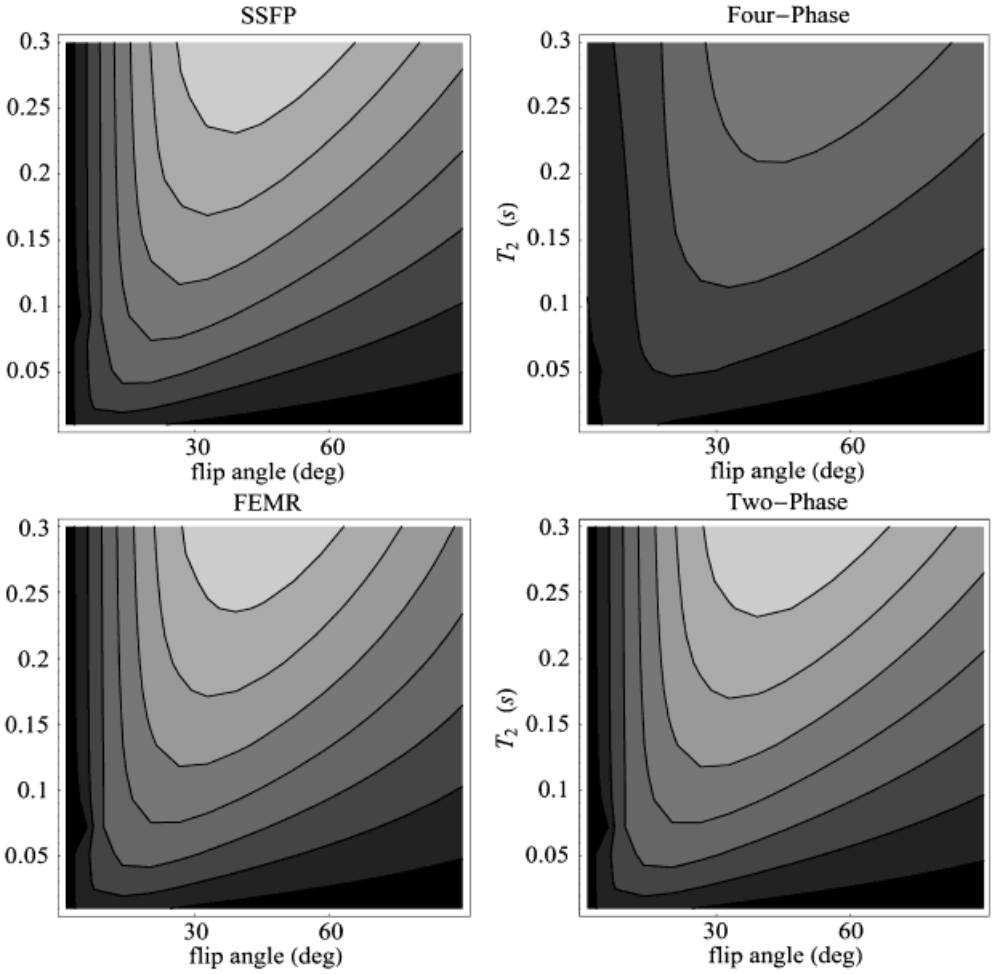

FIG. 5. SNR efficiency of SSFP, four-phase, two-phase, and FEMR imaging (clockwise, starting at upper left). The contour plots above show normalized signal from spins in the middle of the passband of each sequence as a function of flip angle and T_2 for a species with a T_1 of 900 ms, and a TR of 2.5 ms for all sequences. To account for data acquisition differences, the contour plots are of signals divided by the square root of $\alpha = T_s n$, where T_s is the total scan time and n is the number of measurements contributing to each k-space point. Contour levels are in increments of 0.04 with black implying 0–0.04 and white 0.36–0.4.

quences (Figs. 9, 10). In both of these figures, the spectra were determined for sequences with a TR of 3.3 ms, so the signal (vertical axes) as a function of the off-resonance (horizontal axes) should be periodic, with a period of 300 Hz. Though water phantom results in parallel theoretical calculations, lipid phantoms betray an intense signal band in SSFP and two-phase images unanticipated by modeling spin dynamics with the Bloch equations. As mentioned above, spin decoupling between protons in lipids may prolong T_2 relaxation times, thus increasing the lipid signal. However, a suppression band in two-phase images is still present in the lipid images, one broad enough to permit practical lipid suppression.

Water and lipid images can be rapidly obtained with two-phase imaging. The optimal repetition time is 2.2 ms at 1.5 T, separating the centers of the passband and stopband of the spectral profiles of both images by 220 Hz. Note that the lipid image may serve as a mask to suppress

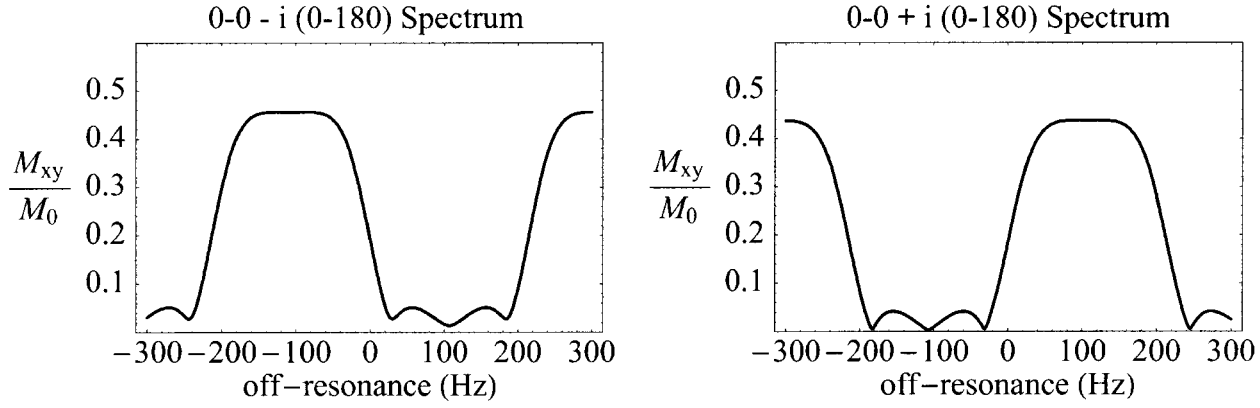

FIG. 6. Two-phase LCSSFP imaging equilibrium signal for sequences with TR = 2.5 ms and a 25° flip angle. Left graph shows spectrum of D_{0-0}–iD_{0-180} for species with T_1 of 340 ms and T_2 of 80 ms, i.e., lipid. Left graph shows spectrum of $D_{0-0} + iD_{0-180}$ for species with T_1 of 900 ms and T_2 of 200 ms, i.e., blood. Note that the two spectra are nearly orthogonal, so images reconstructed from the two linear combinations of data are of spins from two different regions of the spectrum. Hence, one image will be of water protons, the other of lipid protons.

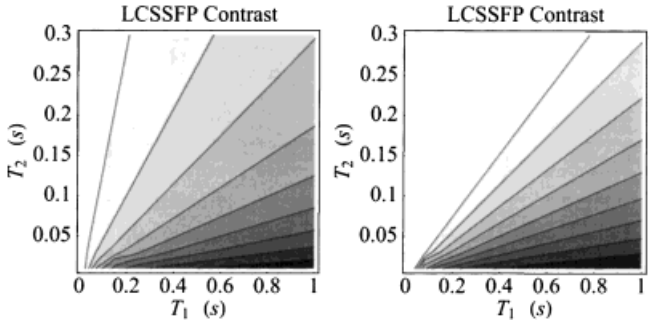

FIG. 7. Two-phase LCSSFP imaging equilibrium signal from spins with resonance frequency in the middle of the passband for sequences with TR = 2.5 ms and linear combination $D_{0–0} + iD_{0–180}$. The left graph shows signal for a sequence with flip angle of 25°, and the right graph shows signal for a sequence with flip angle of 35°. The nearly straight contours of constant signal indicate a T_2/T_1 contrast. However, since most tissues of interest lie in the lower right corner of the graphs, the contrast of two-phase LCSSFP imaging is very similar to T_2-weighting. Note that the relative contributions of T_1 and T_2 to image contrast can be controlled by adjusting the flip angle.

the display of the remaining lipid regions in the predominantly water image (1). Specifically, all pixels in the water image corresponding to the high-intensity pixels in the lipid image can be nulled. Although the method may introduce artifacts when voxels harbor both water and lipid protons, these artifacts may be innocuous in certain applications, such as MR angiography with maximum intensity projections. As an alternative, lipid and water images may be subtracted. As a 3D technique, two-phase imaging may serve well in musculoskeletal imaging applications, particularly to survey rapidly large volumes. Figure 11 is an example demonstrating synovial fluid and cartilage with high and intermediate signal intensities, respectively, in water images, whereas bone marrow and subcutaneous fat are bright in the lipid images. As a 2D technique, two-phase imaging may find a role in abdominal imaging with breathholding. Figure 12 shows axial images of the abdomen; note that the portion of an arm demonstrates lipid suppression even at the edge of the FOV, where inhomogeneities are worst.

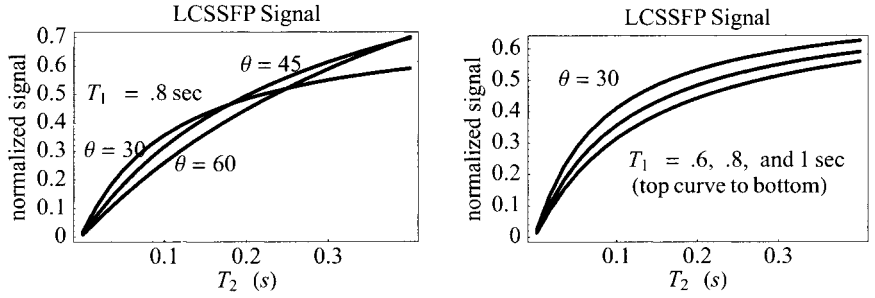

FIG. 8. T_2-weighting of two-phase LCSSFP sequence. Left and right graphs show relative signal with a two-phase LCSSFP sequence for various flip angles and T_1 relaxation times, respectively.

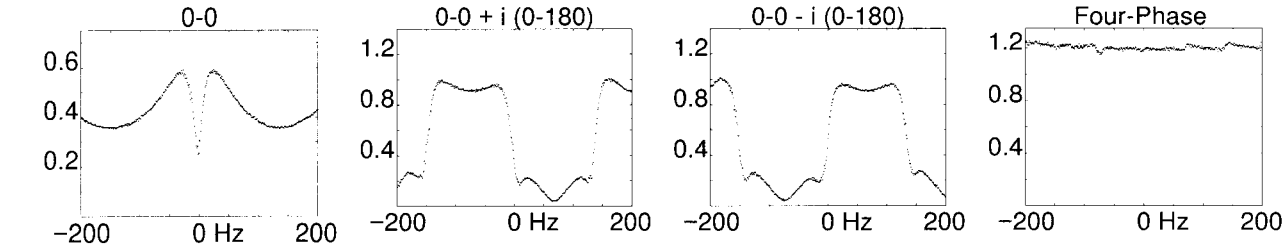

FIG. 9. Average M_{xy} vs. off-resonance of a water phantom, with measured T_1 and T_2 of 82 ms, of (from left to right) SSFP (0–0), LCSSFP with $D_{0–0} + iD_{0–180}$, LCSSFP with $D_{0–0} - iD_{0–180}$, and $D_{0–0–0–0} + D_{0–90–180–270} + D_{0–180–0–180} + D_{0–270–180–90}$. The vertical scale is arbitrary, and all sequences employed a 45° flip angle and 3.3 ms TR.

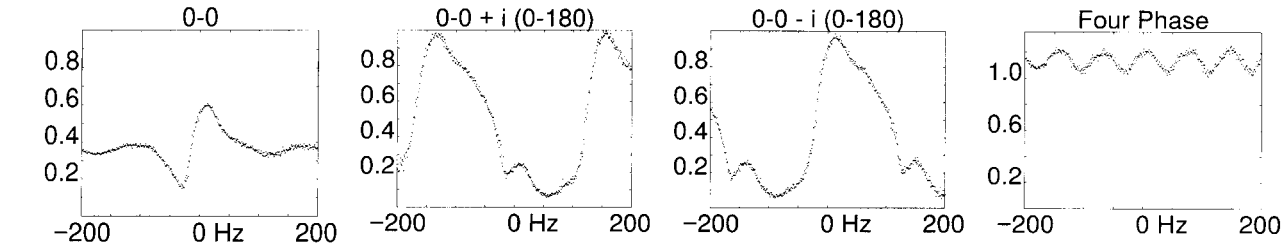

FIG. 10. Average M_{xy} vs. off-resonance of a lipid phantom, with measured T_1 of 165 ms and T_2 of 37 ms, of (from left to right) SSFP (0–0), two-phase LC-SSFP with $D_{0–0} + iD_{0–180}$, two-phase LCSSFP with $D_{0–0} - iD_{0–180}$, and four-phase $D_{0–0–0–0} + D_{0–90–180–270} + D_{0–180–0–180} + D_{0–270–180–90}$. The vertical scale is arbitrary, and all sequences employed a 45° flip angle and 3.3 ms TR. Note the larger ripple in the four-phase spectrum compared with that in the water phantom of Fig. 9.

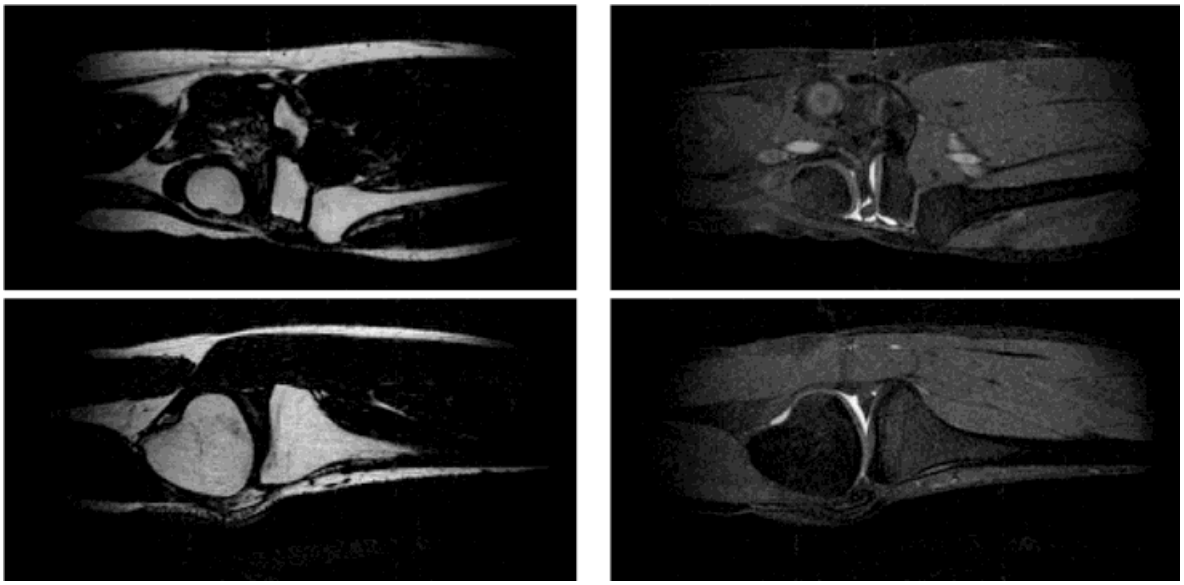

FIG. 11. Sagittal and coronal images from a 3D knee scan using two-phase LCSSFP ($D_{0-0} + iD_{0-180}$ and ($D_{0-0} - iD_{0-180}$) with TR = 2.7 ms, a 26° flip angle, and an extremity coil. A total imaging time for $28 \times 14 \times 14$ cm^3 FOV with 1.1 mm isotropic resolution of 84 sec includes both lipid and water image acquisition time.

Since arterial blood has a relatively long T_2 relaxation time of 220 ms compared with that of muscle, connective tissue and venous blood (35 ms, 35 ms, and 100 ms, respectively), a novel type of flow-independent angiography is possible with LCSSFP (15). A large 3D volume can be rapidly imaged at high resolution, without the expense and trouble of administering a contrast agent. Figure 13, with a maximum intensity projection (MIP) of a 3D image set, shows the feasibility of this application of two-phase imaging. Also seen in the figure is bright synovial fluid of the knee joint, a potential drawback of the technique. As high-SNR lipid images are concomitantly

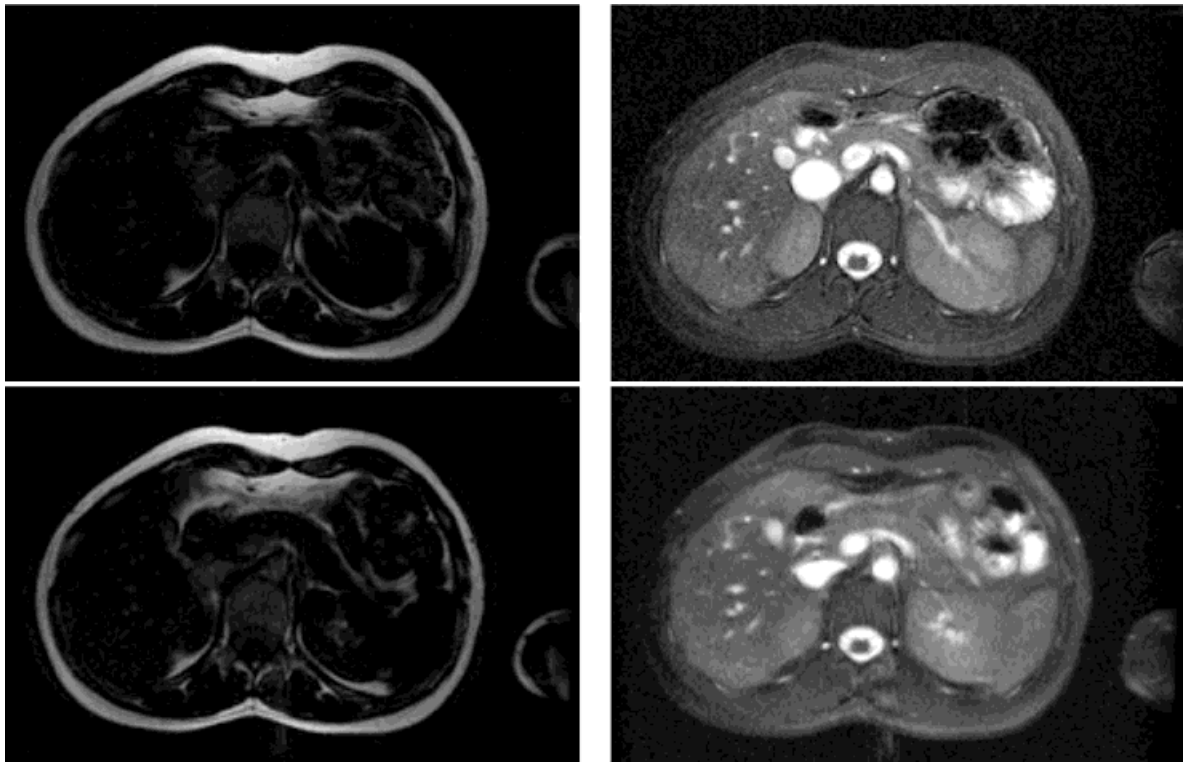

FIG. 12. Cropped axial images from a 2D abdominal scan using two-phase LCSSFP (top images, $D_{0-0} + iD_{0-180}$ and ($D_{0-0} - iD_{0-180}$) and 0–90 FEMR (bottom images) with TR = 2.76 ms, a 45° flip angle, and a torso phased array coil, a 32×32 cm^2 FOV, and 256×256 resolution, and a fractional echo. With a scan time of 1.5 sec per image pair, the left images show predominantly fat, while the right images are mainly water.

FIG. 13. Popliteal artery. Maximum intensity projection (MIP) of 3D image set obtained with the two-phase technique ($D_{0–0} + iD_{0–180}$). Sequence parameters were TR = 2.7 ms, 26° flip angle, 1.1 mm isotropic resolution over 28 × 14 × 14 cm^3 FOV, and 1:24 total scan time.

obtained, atherosclerotic plaque assessment may also be possible.

An application of the four-phase technique is high-SNR brain imaging with T_2-like contrast. Although Fig. 14 shows implementation of the technique as a 2DFT sequence, 3D imaging is also possible, as is non-Cartesian k-space coverage. The SNR of cerebrospinal fluid in the four-phase image in Fig. 14 with 1.25 mm^2 pixels, 7 mm slice thickness, 15-sec scan time per slice is 60, and no banding artifacts are present.

DISCUSSION

We have described a novel method of generating spectral selectivity in SSFP imaging. Two-phase and four-phase imaging are simple processing examples of the technique. Two-phase imaging provides water/lipid discrimination, whereas four-phase imaging yields high SNR images without the banding artifact seen in standard SSFP sequences. In four-phase images of phantoms acquired in the presence of a large shim gradient field, the banding artifact is replaced by seams (Fig. 3). Two mechanisms may be responsible for the seams. The relatively large field variation within a single voxel causes signal cancellation due to phase variation in the equilibrium magnetization. Additionally, this phase variation increases with T_1/T_2, which is nearly unity for the water phantoms in this study. However, these seams are absent from in vivo images acquired without shim fields.

Because free precession sequences maintain transverse coherences, species with long T_2 relaxation times yield relatively high signal. For four such sequences (SSFP, two-phase, four-phase, and FEMR), the optimal flip angle for maximizing contrast of tissues with T_2 relaxation times between 0 and 200 ms is approximately 30°, as can be seen from Fig. 5. However, although the optimal flip angle is the same for all sequences, four-phase and especially two-phase imaging yield greater contrast, whereas FEMR essentially mirrors SSFP in this respect. Neglected in this analysis is magnetization transfer effects, which are significant since all sequences are near the SAR limit.

Additionally, the spectral response of the sequence depends on the T_1 and T_2 of the tissues in the image, along with the flip angle. Thus, the quality of the water–lipid separation depends in part on the flip angle, as illustrated in Fig. 15 with simulated spectra of several tissues with a flip angle of 30°. At −100 Hz, from highest to lowest signal, are synovial fluid (1470 ms T_1, 535 ms T_2) (16), liver (490 ms T_1, 43 ms T_2) (17), spleen (780 ms T_1, 62 ms T_2) (17), cartilage (770 ms T_1, 39 ms T_2) (16), muscle (980 ms T_1, 31 ms T_2) (16), and adipose tissue (300 ms T_1, 80 ms T_2). For lipids, the stopband remains broad when the flip angle is below 35°, and for most other tissues the passband remains broad when the flip angle is above 10°. Hence, although the ''lipid'' image may have a significant water contribution, the ''water'' image will remain relatively free of lipid signal.

The method described in this paper is ideal for imaging long T_2 species, such as blood (angiography, Fig. 13),

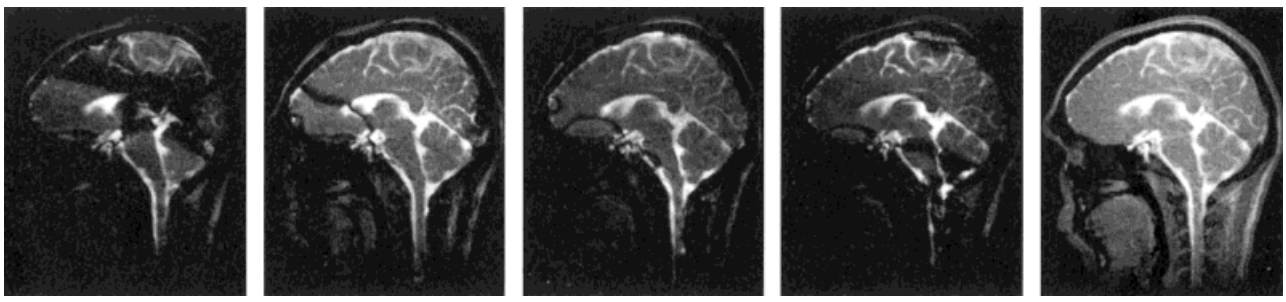

FIG. 14. Cropped sagittal images from a 2D scan with a head coil using standard SSFP (from left to right, $D_{0–0–0–0}$, $D_{0–90–180–270}$, $D_{0–180–0–180}$, and $D_{0–270–180–90}$), and four phase imaging (rightmost image, $D_{0–0–0–0} + D_{0–90–180–270} + D_{0–180–0–180} + D_{0–270–180–90}$). Sequence parameters were TR = 15 ms, a 45° flip angle, 256 × 256 resolution over 32 × 32 cm^2 FOV. The four SSFP images show the characteristic banding artifact, due to field inhomogeneity, whereas the four-phase image betrays no such artifact.

biliary fluid (cholangiography), cerebrospinal fluid (myelography), and joint fluid (Fig. 11). Also, oxygenation measurement and functional MRI can benefit. Fluoroscopic MRI in general, and cardiac fluoroscopy in particular, can take advantage of the method's high speed and signal.

Two-phase imaging provides a unique method of lipid suppression in rapid imaging. Conventional methods of lipid suppression, such as chemically selective saturation (CHESS), exploit chemical shift differences over a single repetition interval. Thus, the duration of RF excitation pulses required to achieve spectral selectivity is determined by the relative chemical shifts of water and lipid protons, a 200 Hz shift at 1.5 T, implying pulses longer than 5 ms. Besides lengthening scan time and reducing SNR efficiency, achieving fat suppression with such a lengthy excitation in a refocused imaging sequence would present severe banding artifacts, since the long excitation pulse enforces a long repetition time. Furthermore, conventional methods require large unrefocused gradients, and are thus incompatible with any refocused imaging sequence. Similarly, spectral-spatial pulses are relatively long in duration. Inversion nulling of lipids is incompatible with the desired steady-state signal from water protons.

Diagnostic situations requiring T_2-like weighting and fat suppression are amenable to the method described in this article, i.e., abdominal, pelvic, and breast MRI. For example, hepatic lesion detection requires T_2-weighted imaging with echo times greater than 80 ms, and lesion characterization necessitates echo times in excess of 120 ms (18). Additionally, the concomitant lipid image may prove particularly useful, as in discrimination between focal sparing in diffuse fatty metamorphosis of the liver and neoplastic involvement. Similarly, comparison of lipid and water images may permit assessment of microscopic and macroscopic fat in adrenal lesions, and hence discrimination of adrenal adenomas from malignancies, as in phase-contrast imaging (19,20).

Additionally, species with a relatively high T_2/T_1 ratio yield high signal. Thus, contrast-enhanced angiography is possible with this fast imaging method; since angiograms can be obtained without contrast (Fig. 13), very low doses of gadolinium may be employed, permitting imaging at multiple stations without exceeding dosing guidelines. Studies of contrast agent uptake kinetics are becoming more common in brain, breast, and abdominal imaging; optimal use requires rapid injection and imaging, since equilibration between intravascular and interstitial spaces can be quick (21,22). Alternatively, fast imaging with T_2 shortening agents, such as superparamagnetic iron oxide, may be useful.

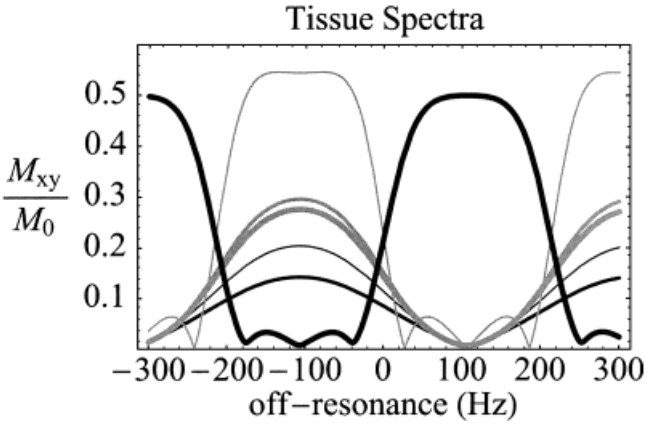

FIG. 15. Spectra of several tissues in two-phase imaging with a 2.5 ms TR and 30° flip angle. From highest to lowest, at −100 Hz are spectra of $D_{0-0} + iD_{0-180}$ for synovial fluid, liver, spleen, cartilage, and muscle, and the spectrum of $D_{0-0} - iD_{0-180}$ for adipose tissue.

Both LCSSFP and FEMR methods provide attractive sequences for fast imaging with T_2-like contrast and lipid/water discrimination. Specifically, two-phase imaging and 0–90 FEMR have similar spectral responses, though the two-phase spectral response stopband has a lower amplitude. Thus, two-phase imaging offers improved lipid/water contrast over FEMR. However, FEMR has several advantages. Because the FEMR technique employs an interleaved acquisition of lipid and water phase encodes, an FEMR image may have fewer motion artifacts than a two-phase image created from combining phase encode data from two SSFP sequences executed sequentially. This FEMR advantage may be of overriding concern in abdominal imaging or studies with time-varying contrast agent concentrations. Additionally, FEMR permits acquisition of the lipid-suppressed image without obtaining data for a lipid image simply by omitting gradient pulses (phase encodes and readouts) after every other excitation. Thus, although the scan time is still double that of SSFP, gradient heating is reduced, expanding applicability to lower performance systems. Two-phase imaging also permits omission of gradient pulses after every other excitation, but the scan time is then four times longer than SSFP. Thus, the improved lipid/water discrimination of two-phase imaging must be weighed against the potentially superior motion insensitivity and gentler gradient demands of FEMR.

The linear combination method is compatible with several readout strategies, including 2DFT, 3DFT, projection reconstruction, echo planar, and non-Cartesian k-space trajectories. However, two-phase imaging demands a short repetition time over which lipid and water spins precess out of phase; four-phase imaging places less demanding constraints on the sequence TR and is compatible with most gradient systems in clinical use today. With the ever-increasing adoption of fast gradient hardware, these techniques will become viable. An alternative strategy of lowering field strength has recently been proposed in the context of SSFP by Duerk et al. (23). For example, at 0.5 T, water/lipid separation is difficult by conventional techniques, such as inversion recovery, spectrally selective excitation, and Dixon methods, but is achieved via two-phase imaging with an optimal repetition time of 6.6 ms, much less demanding than 2.2 ms TRs at 1.5 T. Variants of the LCSSFP method, such as combining SSFP data from sequences with varying flip angles, repetition times, and RF phases are also possible.

CONCLUSION

LCSSFP is a fast, high-signal imaging technique. With different linear combinations of Fourier data from SSFP sequences, several images, each with different spectral selectivity, can be reconstructed. Flexible control of the

relative T_2 contribution to contrast in images is achieved by varying the flip angle of RF excitation. Although very simple in concept and implementation, one variation called two-phase imaging addresses the important problem of incorporating water–lipid discrimination into fast, high-SNR refocussed techniques. Additionally, another variation called four-phase imaging eliminates the banding artifact of SSFP imaging. We have demonstrated the feasibility of several natural applications: musculoskeletal, abdominal, brain, and angiographic imaging.

ACKNOWLEDGMENT

S.S.V. thanks the Medical Scientist Training Program.

REFERENCES

1. Vasanawala SS, Pauly JM, Nishimura DG. Fluctuating equilibrium MRI. In: Proc., ISMRM, 7th Annual Meeting, Philadelphia, 1999. p 4.
2. Schwenk A. NMR pulse techniques with high sensitivity for slowly relaxing systems. J Magn Reson 1971;5:376–389.
3. Zur Y, Wood ML, Nueringer LJ. Motion-insensitive, steady-state free precession imaging. Magn Reson Med 1990;16:444–459.
4. Carr HY. Steady-state free precession in nuclear magnetic resonance. Phys Rev 1958;112:1693–1701.
5. Oppelt A, Graumann R, Barfus H, Fischer H, Hartl W, Shajor W. FISP—a new fast MRI sequence. Electromedica 1986;54:15–18.
6. Hawkes RC, Patz S. Rapid Fourier imaging using steady-state free precession. Magn Reson Med 1987;4:9–23.
7. Jolesz FA, Patz S. Clinical experience with rapid 2DFT SSFP imaging at low field strength. Magn Reson Imaging 1988;6:397–403.
8. Zur Y, Stokar S, Bendel P. An analysis of fast imaging sequences with steady-state transverse magnetization refocussing. Magn Reson Med 1988;6:175–403.
9. Allerhand A. Analysis of Carr-Purcell spin-echo NMR experiments on multiple-spin systems. I. The effect of homonuclear coupling. J Chem Phys 1966;44:1–9.
10. Henkelman RM, Hardy PA, Bishop JE, Poon CS, Plewes DB. Why fat is bright in RARE and fast spin-echo imaging. J Magn Reson Imaging 1992;2:533–540.
11. Williamson DS, Mulkern RV, Jakob PD, Jolesz FA. Coherence transfer by isotropic mixing in Carr-Purcell-Meiboom-Gill imaging: implications for the bright fat phenomenon in fast spin-echo imaging. Magn Reson Med 1996;35:506–513.
12. Ernst RR. Fourier transform NMR spectroscopy employing a phase modulated rf carrier. U.S. Patent Number 1976;3968424.
13. Riederer SJ, Tasciyan T, Farzaneh F, Lee JN, Wright RC, Herfkens RJ. MR fluoroscopy: technical feasibility. Magn Reson Med 1988;8:1–15.
14. Kerr AB, Pauly JM, Hu BS, Li KC, Hardy CJ, Meyer CH, Macovski A, Nishimura DG. Real-time interactive MRI on a conventional scanner. Magn Reson Med 1997;38:355–367.
15. Wright GA, Hu BS, Macovski A. Estimating oxygen saturation of blood in vivo with MR imaging at 1.5T. J Magn Reson Imaging 1991;1:275–283.
16. Duewell SH, Ceckler TL, Ong K, Wen H, Jaffer FA, Chesnick SA, Balaban RS. Musculoskeletal MR imaging at 4 T and 1.5 T: comparison of relaxation times and image contrast. Radiology 1995;196:551–555.
17. Wood ML, Bronskill MJ, Mulkern RV, Santyr GE. Physical MR desktop data. J Magn Reson Imaging 1993;3.
18. Mirowitz SA. Diagnostic pitfalls and artifacts in abdominal MR imaging: a review. Radiology 1998;208:577–589.
19. Mitchell DG, Crovello M, Matteucci T, Petersen RO, Miettinen MM. Benign adrenocortical masses: diagnosis with chemical shift MR imaging. Radiology 1992;185:345–351.
20. Tsushima Y, Ishizaka H, Matsumoto M. Adrenal masses: differentiation with chemical shift, fast low-angle short MR imaging. Radiology 1993;186:705–709.
21. Hamm B, Wolf KJ, Felix R. Conventional and rapid MR imaging of the liver with Gd-DTPA. Radiology 1987;164:313–320.
22. Mirowitz S, Lee JKT, Gutierrez E, Brown JJ, Heiken JP, Eilenberg SS. Dynamic gadolinium-enhanced rapid acquisition spin-echo MR imaging of the liver. Radiology 1991;179:371–376.
23. Duerk JL, Lewin JS, Wendt M, Petersilge C. Remember true FISP? A high SNR near 1-second imaging method for T2-like contrast in interventional MRI at .2 T. J Magn Reson Imaging 1998;8:203–408.